
Proceedings Paper:
Terzioglu, F. orcid.org/0000-0002-2639-2992, Rongong, J.A. and Lord, C.E. (2020) The dissipative characteristics of oblate particles in granular dampers. In: Papadrakakis, M., Fragiadakis, M. and Papadimitriou, C., (eds.) EURODYN 2020: Proceedings of the XI International Conference on Structural Dynamics. EURODYN 2020: XI International Conference on Structural Dynamics, 23-26 Nov 2020, Athens, Greece. European Association for Structural Dynamics (EASD) , pp. 4851-4866. ISBN 9786188507227

10.47964/1120.9393.20452

EURODYN 2020
XI International Conference on Structural Dynamics
M. Papadrakakis, M. Fragiadakis, C. Papadimitriou (eds.)
Athens, Greece, 22–24 June 2020

THE DISSIPATIVE CHARACTERISTICS OF OBLATE PARTICLES IN GRANULAR DAMPERS

Furkan Terzioglu[1], **Jem A. Rongong**[1], **and Charles E. Lord**[1]

[1] The University of Sheffield, Department of Mechanical Engineering
Mappin Building, Mappin Street, Sheffield, S1 3JD, United Kingdom
fterzioglu1@sheffield.ac.uk, j.a.rongong@sheffield.ac.uk, c.lord@sheffield.ac.uk

Keywords: granular damping, friction, impact, irregular particle, sphericity, circularity, discrete element method.

Abstract. *In numerical models for granular dampers, particles are generally considered to be perfect spheres. However, in practical engineering applications these particles can slightly deviate from being true spheres. It has been observed experimentally that sphericity, which defines the proximity degree of a shape to a sphere, plays an important role in the amplitude dependent behaviour of granular dampers. This paper mainly examines the significance of the sphericity level for slightly oblate particles in a granular damper that are subjected to sinusoidal vibrations in the same direction as standard gravity. This investigation is carried out by evaluating the dissipated power from the granular medium by utilizing three-dimensional discrete element method simulations. Apart from the effect of amplitude of vibrations in the dissipated power, the relative contributions of frictional and inelastic collisional damping mechanisms in the overall power dissipation, are also investigated for varying sphericity levels of the oblate particles.*

1 INTRODUCTION

Granular (or particle) damping is an effective passive damping approach that involves many small spherical particles (typically 0.05 mm – 5 mm in diameter) located inside an enclosure that is fixed to a vibrating structure. The kinetic energy from vibration is transmitted to the particles by collisional momentum exchanges between the particles and the boundaries of the enclosure. Granular dampers dissipate the transmitted kinetic energy through inter-particle and particle-enclosure boundary interactions. This is unlike common viscoelastic dampers which generally dissipate the stored elastic energy.

Interest in granular damping is rapidly increasing in engineering fields because such dampers are robust, cost-effective, easy to retro-fit and relatively insensitive to the environment and excitation frequency. [1–4]. As a result, granular dampers have been successfully applied in numerous mechanical systems to solve noise and vibration problems, such as a desk-top banknote processing machine [5], the exterior panel of a launch vehicle [6], a gear transmission system [7], and an automotive oil pan [8].

Despite their conceptual simplicity, granular dampers have quite complex and distinctive behaviour. Since the particles are generally hard, made from materials such as metal and ceramic, surface friction plays an important role in energy dissipation, which leads to significant non-linearity in the form of amplitude dependent behaviour [9,10]. Granular damping has been studied extensively and this non-linearity is the likely reason for the existence of many contradictory findings in the literature. To improve understanding, studies have been undertaken to investigate the sensitivity of granular damping against damper parameters, such as coefficient of restitution between impacting bodies, coefficient of friction in contacting surfaces, particle number and individual stiffness of particles and enclosure walls [11–13]. More recently, it has also been shown that an approximated granular damper model in Discrete Element Method (DEM) simulations can adequately represent the essential properties of a real granular damper without matching parameters exactly provided the total mass is represented accurately [14]. This presumably arises from the compensation feature of multiple particles against the small variations of parameters from exact ones. It should be noted that this 'universal response' approach is only valid when using relatively large numbers of particles.

Previous studies have reported that granular dampers exhibit the characteristic properties of both friction dampers and single impact dampers since the main damping mechanisms of granular dampers are surface friction and inelastic collision within the granular media [15]. Furthermore, it has been also emphasized before that understanding of the damping mechanisms would provide an efficient way to increase the performance of such dampers [1]. Accordingly, a few attempts have been made to identify relative contributions of damping mechanisms in granular damping [15–18]. However, much uncertainty still exists and the literature on this topic is very scarce.

Although the hard particles used in granular dampers typically have a high level of durability, over time their shape may deviate from a true sphere due to harsh working conditions or intense collisional events. Moreover, non-spherically shaped particles may be deliberately used either for cost reasons or to avoid practical design issues such as the packing problem in small voids or because of manufacturing tolerances. Therefore, the investigation of irregular particles has grown in importance [19–21]. However, there is no notable study that focuses upon slightly oblate particles in granular dampers.

The aim of this study is to provide a numerical investigation on slightly oblate hard particles in a granular damper undergoing harmonic vibrations in the same direction as gravity. Several three dimensional DEM simulations are carried out to find the effects of particle sphericity levels on the dissipative behaviour. Steady-state cumulative power loss calculations are

utilized to characterize the amplitude dependent granular damper in every simulation. The contributions of frictional and collisional energy dissipation mechanisms on the total dissipation are computed.

2 DEM MODEL FOR OBLATE PARTICLES

DEM is a numerical scheme for analyzing granular matter, in which the motion of every particle is tracked in time. The full time history of interest is broken into a series of very short time steps over which the equations of motion for each particle are solved. Where particles interact with one another, or with the physical boundaries of the system being studied, appropriate force-displacement and force-velocity relations for the contact are employed. The fundamental theory of DEM was originally presented by Cundall and Strack [22] and was first applied to granular dampers more than 20 years ago [23]. The use of DEM is attractive in the study of granular damping because it provides a way to control and observe the contact parameters and their effect on overall damping achieved.

2.1 Oblate particle generation

Although several algorithms have been developed recently that allow irregular particles to be defined and used directly within the DEM field, the most common method is the multi-sphere approach. In this approach, two or more overlapping spherical particles are rigidly joined together. Relatively complex shapes can be produced as the spheres are allowed to intersect each other. The use of the sphere as the building block provides computational benefits including the existence of advanced contact detection algorithms and contact models. Thus, the oblate particles used in this study are formed by employing the multi-sphere approach in the EDEM 2020 software [24].

Shape is an important indicator which defines a particle in numeric computational fields – especially for rock-like irregular particles [25]. If a large number of spheres is used in the multi-sphere approach, non-spherical shapes can be represented more precisely. However, it also causes significant increases in computational times. Hence, irregular shapes should be modeled conducting a balance between computational efficiency and closeness of representation. In this study, oblate particles are generated considering these criteria and are shown in Figure 1.

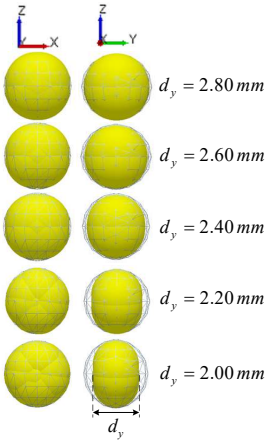

Figure 1: Created particle types for simulations with respect to a $3\,mm$ diameter perfect sphere mesh template.

It should be noted that the reference perfect sphere diameter used in this study is 3 mm and particle resizing occurs along the local y-axis (i.e. d_y changes) as can be seen in Figure 1,

whilst the other lengths (d_x , d_z) are kept constant. In this investigation, the lower limit for d_y was set at 2 mm, which represents a moderate change in particle shape.

The relative similarity of oblate particles to the reference sphere can be described using the sphericity index [25] which can be written as,

$$\psi = \sqrt[3]{\frac{c^2}{ab}} \tag{1}$$

Here, a , b and c are the corresponding lengths (largest to smallest, respectively) along the three local axes. In this paper, only the smallest length of the oblate particles is adjusted and therefore, $c = d_y$, $a = b = d_x = d_z = 3\,\text{mm}$.

Since oblate particles are created by deforming a sphere along one axis, a two dimensional parameter called the circularity index can also be used to define the shape. Circularity is defined in the local YZ axis as shown below [20].

$$C = \sqrt{\frac{4\pi A_{YZ}}{P_{YZ}{}^2}} \tag{2}$$

where A_{YZ} and P_{YZ} are respectively the projection area of a particle on the YZ axis and the perimeter of the particle. Sphericity and circularity values for the oblate particles used in this work, are presented in Table 1.

Particle minor axis length, d_y [mm]	Sphericity, ψ [-]	Circularity, C [-]
2.00	0.763	0.970
2.20	0.813	0.980
2.40	0.862	0.989
2.60	0.909	0.995
2.80	0.955	0.999
3.00	1.000	1.000

Table 1: Shape parameters of oblate particles.

2.2 Contact force model

In DEM, although particles are created as completely rigid bodies, contacts between them are deformable. Contacts are traditionally modeled using spring and dashpot elements as shown in Figure 2a, which allow relatively rapid calculations to be performed. For perfect spheres, force-displacement relationships have already been defined and tested for suitability [26–28]. As the multi-sphere is employed, these validated models can be applied to address the load-deformation behaviour of oblate particles. The contact model used in EDEM 2020 for this study is briefly summarized below considering the spheres shown in Figure 2a.

Normal elastic force between the spheres is determined using the well-known non-linear Hertzian contact model.

$$\boldsymbol{F}_{N_e} = -\underbrace{\frac{4}{3} E^{eq} \sqrt{R^{eq}}}_{k_N} \delta_N{}^{3/2} \boldsymbol{e}_N \tag{3}$$

Here, $\boldsymbol{e}_N$ is the unit vector from the centre point of sphere under consideration to the contact point and δ_N is the normal overlap of sphere. In this expression, the equivalent elastic modulus (E^{eq}) and the equivalent radius (R^{eq}) can be found by $1/E^{eq} = \left(1-\nu_1^2\right)/E_1 + \left(1-\nu_2^2\right)/E_2$ and $1/R^{eq} = 1/\mathrm{R}_1 + 1/\mathrm{R}_2$, where E, R and ν are elastic modulus, radius and Poisson's ratio of relevant spheres, respectively. In order to define inelastic (i.e. dissipative) part of normal force between the spheres, a coefficient of restitution (e) based approach is employed [29]:

$$\boldsymbol{F}_{N_d} = -\underbrace{2\sqrt{\frac{5}{6}}\frac{\ln(e)}{\sqrt{\ln^2(e)+\pi^2}}\left(2m^{eq}E^{eq}\sqrt{R^{eq}\delta_N}\right)^{1/2}}_{c_N}\frac{d\boldsymbol{r}_{\boldsymbol{rel}_N}(t)}{dt} \tag{4}$$

where equivalent mass (m^{eq}) is defined using the individual masses of spheres $1/m^{eq} = 1/m_1 + 1/m_2$ and $d\boldsymbol{r}_{\boldsymbol{rel}_N}(t)/dt$ denotes the normal relative velocity between the spheres in contact.

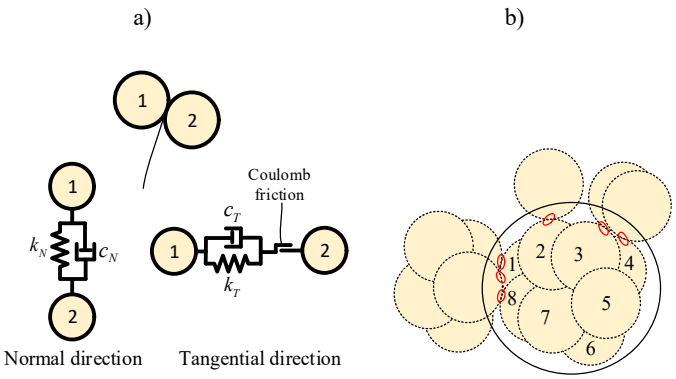

Figure 2: a) Modelling at the contact point of two contacting spheres, b) contacts of an irregular particle constructed with many spheres.

On the other hand, tangential elastic force is determined according to normal overlap defined as Mindlin and Deresiewicz method [16]. Unlike the original method in which many incremental elastic-plastic loading and unloading steps exist [30], a simplified version of this method is used to define tangential elastic force-displacement relation as given below.

$$\boldsymbol{F}_{\boldsymbol{T}_e} = -(1-\vartheta)\underbrace{8G^{eq}\sqrt{R^{eq}\delta_N}}_{k_T}\delta_T\boldsymbol{e}_{\boldsymbol{T}} \tag{5}$$

While equivalent shear modulus (G^{eq}) is defined by $1/G^{eq} = \left(1-\nu_1^2\right)/G_1 + \left(1-\nu_2^2\right)/G_2$ with shear modulus of spheres (G), δ_T and $\boldsymbol{e}_{\boldsymbol{T}}$ stands for the tangential overlap and the unit vector along tangential overlap, respectively. Additionally, tangential inelastic force can be also formed using the similar approach as for normal direction. However, shear friction should be also taken into consideration in tangential direction. Thus, the widely used Coulomb friction model is added to tangential contact model:

$$\boldsymbol{F}_{\boldsymbol{T}_d} = -(1-\vartheta)\underbrace{2\sqrt{\frac{5}{6}}\frac{\ln(e)}{\sqrt{\ln^2(e)+\pi^2}}\left(8m^{eq}G^{eq}\sqrt{R^{eq}\delta_N}\right)^{1/2}}_{c_N}\frac{d\boldsymbol{r}_{\boldsymbol{rel}_T}(t)}{dt} - \vartheta\gamma_f\left|\boldsymbol{F}_{\boldsymbol{N}}\right|\boldsymbol{e}_{\boldsymbol{T}} \tag{6}$$

where $d\boldsymbol{r}_{rel_T}(t)/dt$ is the tangential relative velocity between the spheres and γ_f is coefficient of friction. ϑ is for indicating whether slipping occurs or not as seen in Equation 7.

$$\vartheta = \begin{cases} 1 & |\boldsymbol{F}_T| > \gamma_f |\boldsymbol{F}_N| \\ 0 & otherwise \end{cases} \tag{7}$$

It should be also noted that although the contact model is presented considering sphere – sphere contacts, it would be also valid for sphere – cylindrical enclosure contacts if one assumes $R_{enclosure} \to \infty$ and $m_{enclosure} \to \infty$ in above expressions.

For an irregularly shaped particle modelled using multi-sphere approach, contact force calculation procedure should be performed accounting all existing contacts of all individual spheres which constitute the particle. For example; as can be seen in Figure 2b, 8 perfect spheres which form the irregular particle have different number of contacts with other particles (e.g. number 1 has 2 contacts while number 8 has 1 contact) and the effects of the total 6 contacts can be only obtained by looking all 8 spheres. Thus, the resultant force acting on the particle can be computed as follows for a particle:

$$\boldsymbol{R}_F = \sum_i \left\{ \sum_{j(i)} \left(\boldsymbol{F}_{N_e} + \boldsymbol{F}_{N_d} + \boldsymbol{F}_{T_e} + \boldsymbol{F}_{T_d} + \boldsymbol{F}_g \right) \right\} \tag{8}$$

where i and $j(i)$ are the indices which count the total spheres forming the particle and the total contacts involved by sphere i, respectively. $\boldsymbol{F}_g$ is the gravitational force acting on the corresponding sphere. The resultant moment acting on the particle can be also determined by vectorial product of the resultant force and the position vector of particle mass center ($\boldsymbol{r}_c$).

$$\boldsymbol{R}_M = \boldsymbol{r}_c \times \boldsymbol{R}_F \tag{9}$$

2.3 DEM simulation procedures

In three dimensional DEM simulations, detected contacts of particle – particle and particle – enclosure pairs are considered to perform the given contact force computation procedure at a solution time step. After the calculation of resultant forces and moments, Euler-Newton equations of motions are numerically solved to find updated translational and rotational kinematics (i.e. positions, velocities and accelerations) of every particle by utilizing central-difference formulae.

The time step needs to be set small enough to capture particle overlaps, avoid propagating disturbances of a particle far from away and decrease numerical inaccuracies in simulations. Although several other approaches have been available to estimate a time step for realistic simulations in DEM, the Rayleigh time step criterion is used in the present study [31]. The time interval used in the simulations is chosen to be approximately %50 – %35 of the Rayleigh time step according to the particle type to ensure the reliability of simulations.

Even though there have been studies which investigate the characteristics of granular damping considering the dynamics of host structure [12,32], it is useful to carry out investigations on the damper alone to determine energy dissipation behaviour independently from the host structure [33,34], so that the damper can be adopted to any structure. This study involves a cylindrical enclosure filled with oblate particles subjected to vertical sinusoidal vibrations.

Particles are given the properties of stainless steel while the material of enclosure is chosen as polymethylmethacrylate (PMMA). The properties of these materials and the dimensions of

the enclosure are given in Table 2. The contact properties used in the simulations (i.e. friction and restitution coefficients) are determined as presented in this table. These parameters are selected according to a comprehensive study in which stainless steel – stainless steel and PMMA – stainless steel interactions were experimentally examined to extract the contact properties between those for DEM simulations [35].

Enclosure parameters		**Particle parameters**	
Material	PMMA	Material	Steel
Elastic modulus	3.3 GPa	Elastic modulus	206 GPa
Poisson's ratio	0.37	Poisson's ratio	0.30
Diameter	0.02 m	Density	7800 kg/m^3
Height	0.04 m	Nominal total mass	0.04 kg
Other simulation parameters			
Particle-enclosure friction coefficient	0.4		
Particle-particle friction coefficient	0.4		
Particle-enclosure restitution coefficient	0.92		
Particle-particle restitution coefficient	0.92		
Time step	~5x10^{-7} s		

Table 2: Parameters and properties of numerical simulations.

To allow a comparative study to be undertaken, it was considered desirable that the total mass of particles remained the same for different particle types. In order to achieve a suitable clearance level (75% – 80% filling ratio or 20% – 25% clearance ratio) for practical damping in every simulation configuration [11], the total particle mass was set to 0.04 kg. However, because particles are discrete but had different sizes, the total mass varied by up to the mass of half a particle, as shown in Figure 3a. Figure 3a also shows that a greater deviation in shape from a perfect sphere results in an increase in the number of particles required to achieve the target mass. Before any vibrational loading was applied, all particles were allowed to settle in the enclosure by the gravitational effect (see Figure 4).

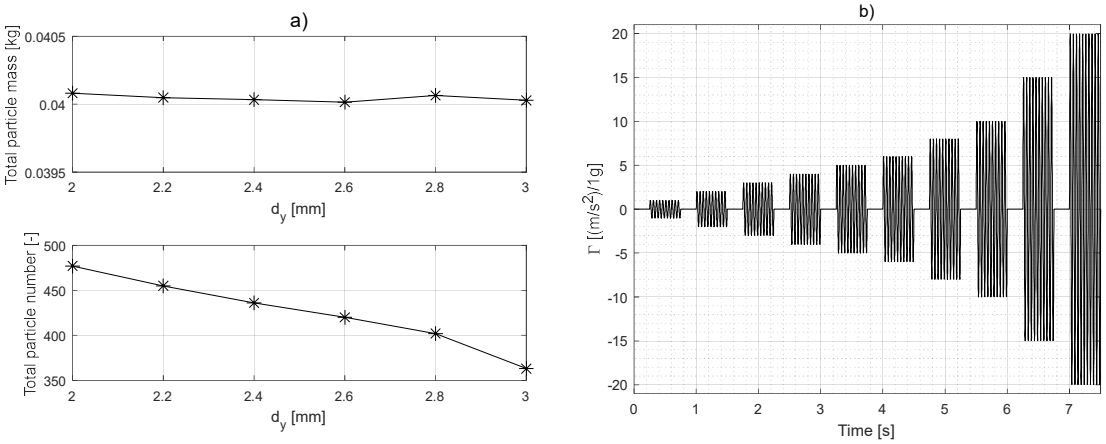

Figure 3: a) Changes in total particle mass and total particle number in terms of particle type, b) given vibration signal.

Behaviour of the granular medium under steady-state vibration was studied by prescribing sinusoidal motion for the enclosure at a frequency of 20 Hz. The effect of vibration intensity

was investigated by increasing the amplitude in steps, with the response being calculated for ten cycles at each level, as shown in Figure 3b. These vibrational levels are represented by commonly used non-dimensional acceleration (Γ).

$$\Gamma = \frac{A\omega^2}{g} \tag{10}$$

where A and ω are displacement magnitude and angular frequency of vibrations, respectively. In the vibration signal, time gaps are provided between each vibrational level to let the particles become stationary before the next excitation.

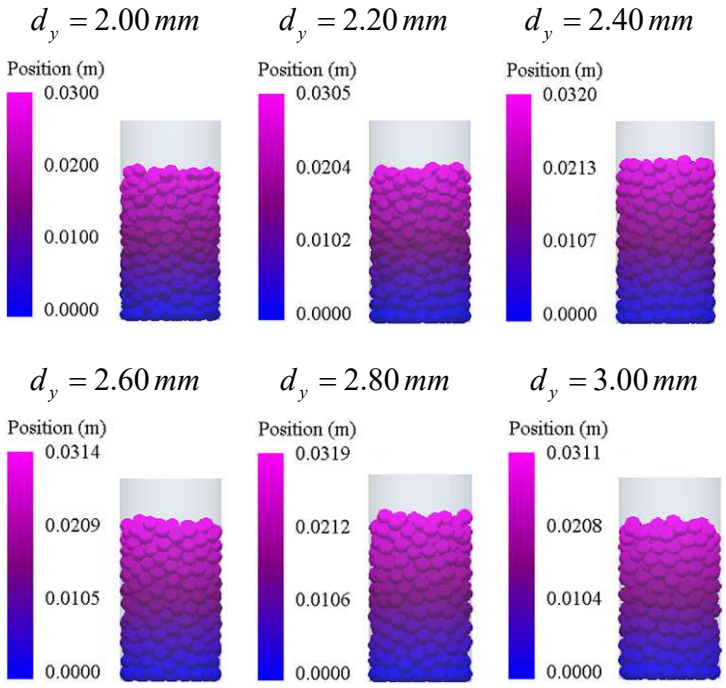

Figure 4: Views of granular oblate particles in the enclosure after settling process (i.e. stationary positions).

3 DISSIPATED ENERGY CALCULATION

Total cumulative dissipated energy in the simulations can be obtained by utilizing an incremental numeric computation scheme. For a single contact, total dissipated energy increments (ΔE_C) are computed integrating the scalar product of dissipative forces (i.e. in normal direction, $\boldsymbol{F}_{N_d}$ and in tangential direction, $\boldsymbol{F}_{T_d}$) and corresponding relative velocities between the contacting bodies through the contact time, T_c. In order to account all N number of contacts in the current computation step, this calculation is repeated for every contact, and then the effects of every contact is summed accordingly as following.

$$\Delta E_C = \sum_{k=1}^{N} \int_{T_c^{(k)}} \left\{ \left| \boldsymbol{F}_{N_d}^{(k)}(t) \cdot \frac{d\boldsymbol{r}_{rel_N}^{(k)}(t)}{dt} \right| + \left| \boldsymbol{F}_{T_d}^{(k)}(t) \cdot \frac{d\boldsymbol{r}_{rel_T}^{(k)}(t)}{dt} \right| \right\} dt \tag{11}$$

where $\boldsymbol{r}_{rel_N}$ and $\boldsymbol{r}_{rel_T}$ represent the relative positions of contacting bodies with respect to each other in normal and tangential directions, respectively, while t stands for time. In addition, the computation time step of the energy dissipation calculation scheme should be sufficiently larger than the contact durations to account all contacts within a single step.

The tangential dissipation can arise from either friction between the bodies in contact or restitution of the bodies unlike the normal dissipation where whole dissipation is caused by only collisional restitution. Frictional dissipation is solely employed if slipping, in which the tangential force is higher than the maximum static friction force between the contacting bodies, is occurred. The frictional cumulative dissipation steps can be separately determined as given in below.

$$\Delta E_C^f = \gamma_f \sum_{k=1}^{N} \int_{T_c^{(k)}} \left| \boldsymbol{F}_N^{(k)}(t) \cdot \frac{d\boldsymbol{r}_{\boldsymbol{rel}_T}^{(k)}(t)}{dt} \right| dt \tag{12}$$

Collisional dissipation can then be obtained by subtracting the frictional loss from the total dissipation energy.

$$\Delta E_C^c = \Delta E_C - \Delta E_C^f \tag{13}$$

4 RESULTS

4.1 Overall dissipative behaviour of oblate particles

To assess the general damping behaviours of oblate particles against different vibrational amplitudes and the relationship between the dissipation and the granular motional behaviour, cumulative total dissipated energies were extracted separately for every vibrational case in all simulations. Figure 5 presents some of those dissipated energy results. In these results, the last five vibration periods at each vibration level are considered. Simulations were repeated to determine the effects of packing on the results. The results verified that packing effects stay very small except at the amplitude $\Gamma = 1$.

The first set of analyses belongs to very small oscillations (i.e. $\Gamma = 1.0$). Under such small vibrations, the particles inside the enclosure have almost no relative motions with respect to each other, they only follow the enclosure motion (i.e. solid-like behaviour) since the particles do not overcome the gravitational and the static frictional forces within the granular media. Thus, the dissipated energies are extremely small, and they do not exhibit obvious steady-state behaviors since a few individual particle movements that induce energy dissipation can be instantly observed due to wave propagation through the granular media from the bottom boundary of the enclosure. These instantaneous dissipation increases can be more likely seen for perfect spheres owing to their smooth circular surfaces. In addition, numerical errors in computational operations and initial packing may also considerably affect these small outcomes.

It is apparent from Figure 5 that huge differences surprisingly emerge between the particle types at several vibration amplitudes. Further investigation into granular media indicates that this is mainly connected with the dissimilarities of granular motional states which the particles are in. For instance; in Figure 5d, there are two groups of result: one is high dissipation group, and the other is low dissipation. At this vibration level, the high energy dissipation group is at the onset of two-sided bouncing bed behaviour in which the granular particle cluster impacts the bottom and the top boundaries of enclosure during a period of vibration (i.e. 2 collective impacts with the enclosure in a period), thereby transferring the momentum effectively to the granular media. On the other hand, the granular media in low dissipation group generally collides with only the bottom boundary in a vibration period (one-sided bouncing bed), while it slightly touches to the top boundary in this period (mild collision).

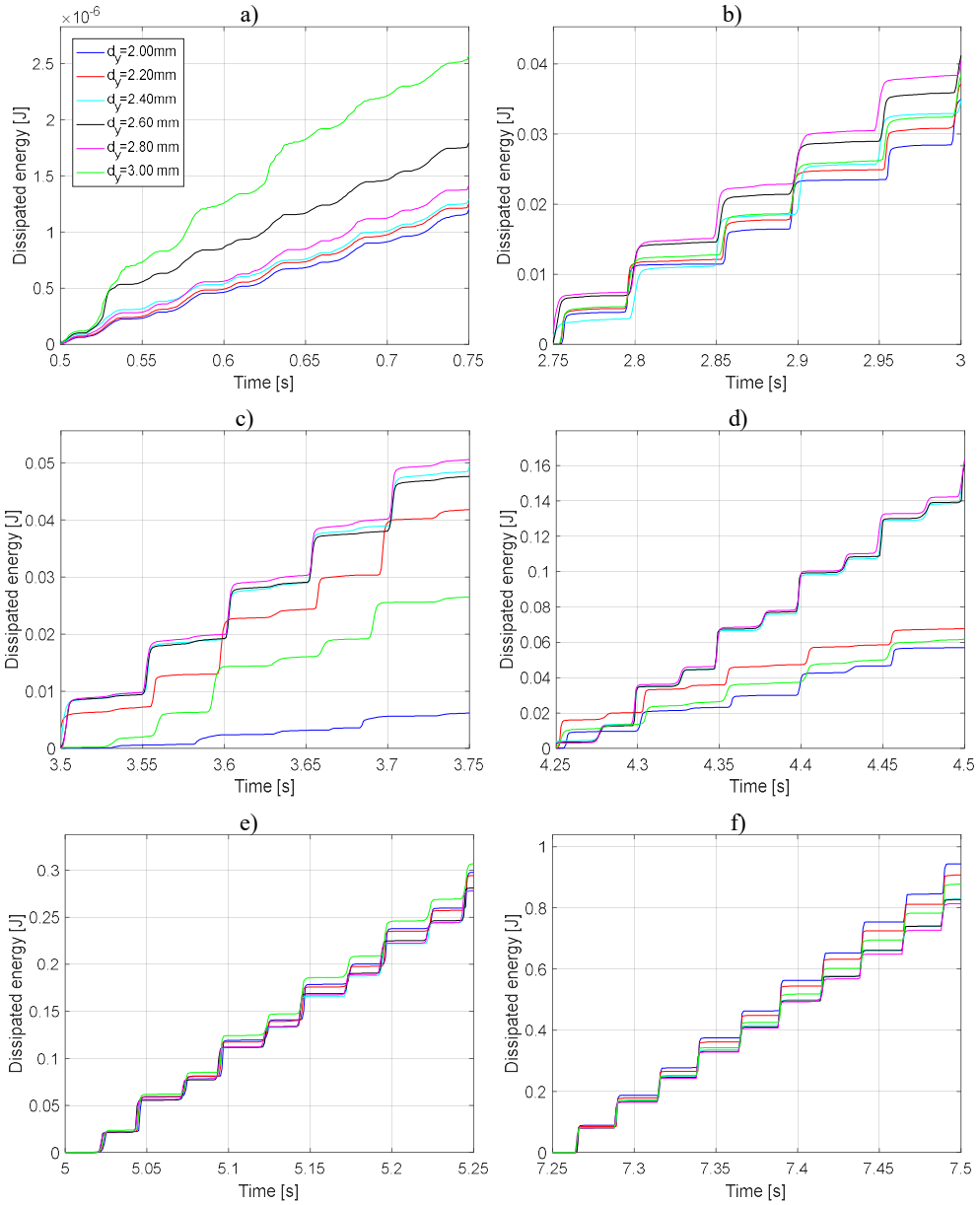

Figure 5: Total cumulative dissipated energy characteristics for 5 vibrational periods of a) $\Gamma = 1$, b) $\Gamma = 4$, c) $\Gamma = 5$, d) $\Gamma = 6$, e) $\Gamma = 8$, f) $\Gamma = 10$.

The defined dissipation groups in Figure 5d are also valid at $\Gamma = 5$ as can be seen in Figure 5c. At this vibration level, the high dissipation group members exhibit similar behaviour to that seen previously except that the granular cluster impacts the top boundary once in every two periods. Although the members of low dissipation group have similar motion, the most squashed particle type somehow executes impacts with quite less intensive than the other members as can be clearly seen in Figure 5c.

Figure 6 shows the total potential energy in the particles throughout the simulation. Observed motional behaviours of granular media at various vibrational sequences are marked with different colors. Purple represents solid-like behaviour, while magenta and cyan stand for one-sided bouncing bed with fluidization of a few of the particles on the top layer and one-sided bouncing bed with fluidization of the uppermost layers of particles, respectively. As one can see in this figure, red marked potential energy regions are clearly more uneven and scat-

tered than other vibrational cases. This result may be explained by the fact that the granular media shows relatively higher level of fluidization in which a reasonable amount of particle indistinctly floats in these loading ranges. Another possible reason for this is that the collective motion of granular media is not symmetric at every vibrational period in these cases as it is in other vibration scenarios. The motions within these red marked ranges are described as following: dotted red is one-sided complete bouncing bed with few individual top particles-top wall impacts in every period, dot-dashed red is one-sided complete bouncing bed with few individual top particles-top wall impacts once in every two periods, dashed red is one-sided complete bouncing bed and mild collective collision with the top wall once in every two periods and flat red is one-sided complete bouncing bed and mild collective collision with the top wall in every period. The last phenomena observed in the simulations is two-sided complete bouncing bed that is marked with blue in total potential energy plots.

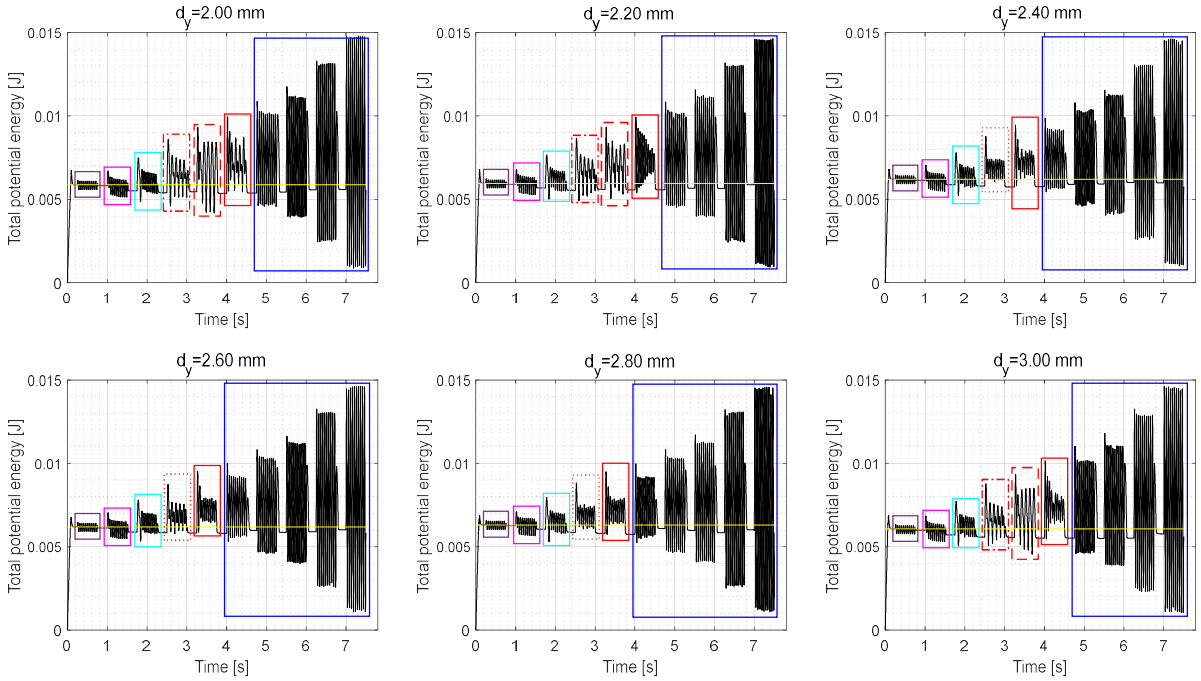

Figure 6: Total potential energy changes of simulated particles in time, yellow flat line indicates the total potential energy at the stationary positon of particles.

4.2 Damping characterization of oblate particles

In order to compare the damping behaviour of oblate particle types, the energy dissipation rates in a steady-state vibration period (i.e. power loss) were determined by integrating the cumulative dissipated energies through this period.

$$Power\,loss = \frac{1}{T}\int_{T} E_C(t)\,dt \tag{14}$$

The power losses are illustrated with respect to either sphericity or circularity for every simulated vibrational level in Figure 7 and Figure 8, respectively. The perfect sphere results are also included in these figures as a reference of default particle type used in most typical granular damper applications. In these graphs, the contribution of damping mechanisms of granular damping (i.e. friction and impact) on overall power loss are also shown to illustrate the macroscale damping behaviour of oblate particles. In addition to this, particle-particle and

particle-enclosure frictional losses are separately depicted in these plots to show dominance of interaction type.

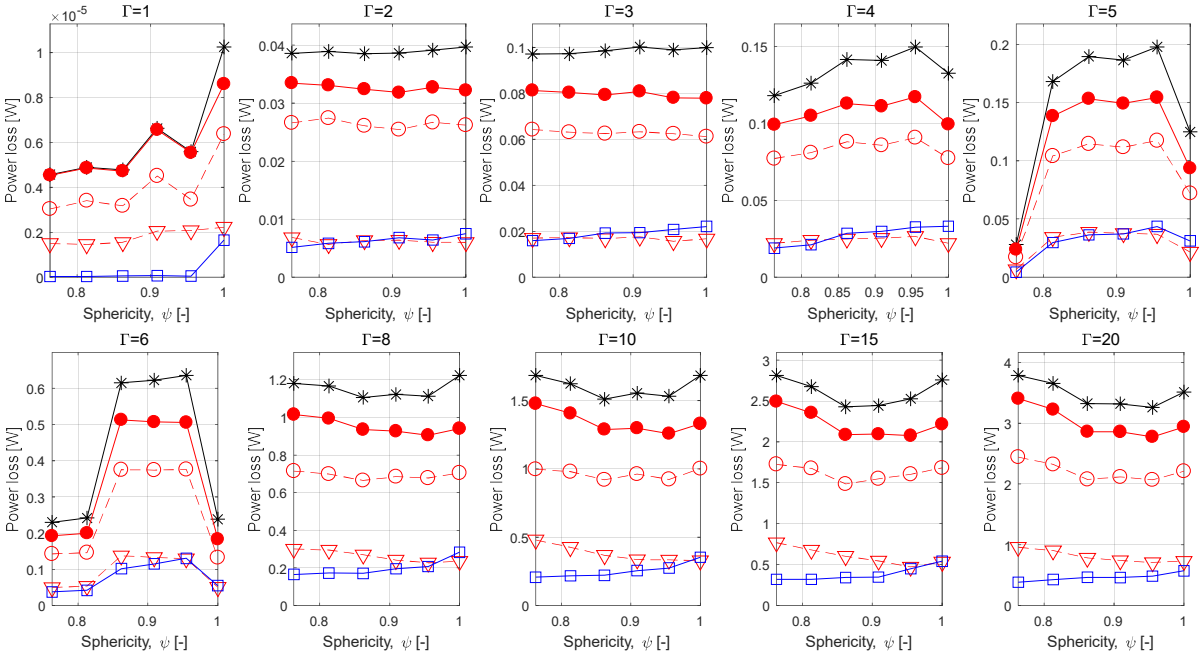

Figure 7: Power loss changes in terms of sphericity at different vibration levels: total loss (—✳—), frictional loss (—●—), inter-particle frictional loss (—⊖—), particle-enclosure frictional loss (—▽—), collisional loss (—□—).

If one looks into the total power loss results omitting the reference particle (i.e. the perfect sphere: $\psi = 1$ and $C = 1$) in both charts, it can be found that there are three damping regimes according to the vibrational intensity in which the total loss is affected by particle shape. The first one is 'inclining' regime where the total power loss generally increases with increasing sphericity or circularity level before $\Gamma \approx 5$. This increasing behaviour becomes moderate at higher amplitudes, whilst it is very slight for small vibrations. Afterwards, there is 'transition' regime up to $\Gamma \approx 8$. Although increasing tendency in total power loss continues in this regime, a dramatic jump is also observed because of impacts with the upper surface of the cavity, as discussed in the previous section. The last damping regime is 'declining' in which the power loss is decreasing with increasing sphericity or circularity unlike the other regimes and this falling behaviour is more apparent at higher vibration amplitudes. Together, these findings suggest that damping is optimised at different amplitudes, depending on particle shape. The results also indicate that there is an oblate particle type which provides more damping than the perfect sphere for almost all vibrational levels. Thus, it can be preferable in granular applications to use very slight oblate particle if the vibrations ensure working before two-sided complete bouncing bed. Otherwise, in two-sided complete bouncing bed state, it is more appropriate to employ highly flattened particles. However, it should be noticed that these results need to be supported by quantitative data from experimental works.

For a given non-dimensional acceleration level, it can be highlighted from the power loss plots that the most dominant damping mechanism is friction for every particle type. Besides, particle-particle frictional interactions are responsible for most of frictional dissipation. In fact, it is reported that particle-particle contacts contribute most of overall dissipation (i.e. particle-enclosure boundary interactions have minor effects on dissipation) as similarly mentioned before [18]. The dominancy of frictional loss leads that the overall damping behaviour stated in the previous paragraph completely reflects the frictional energy dissipation.

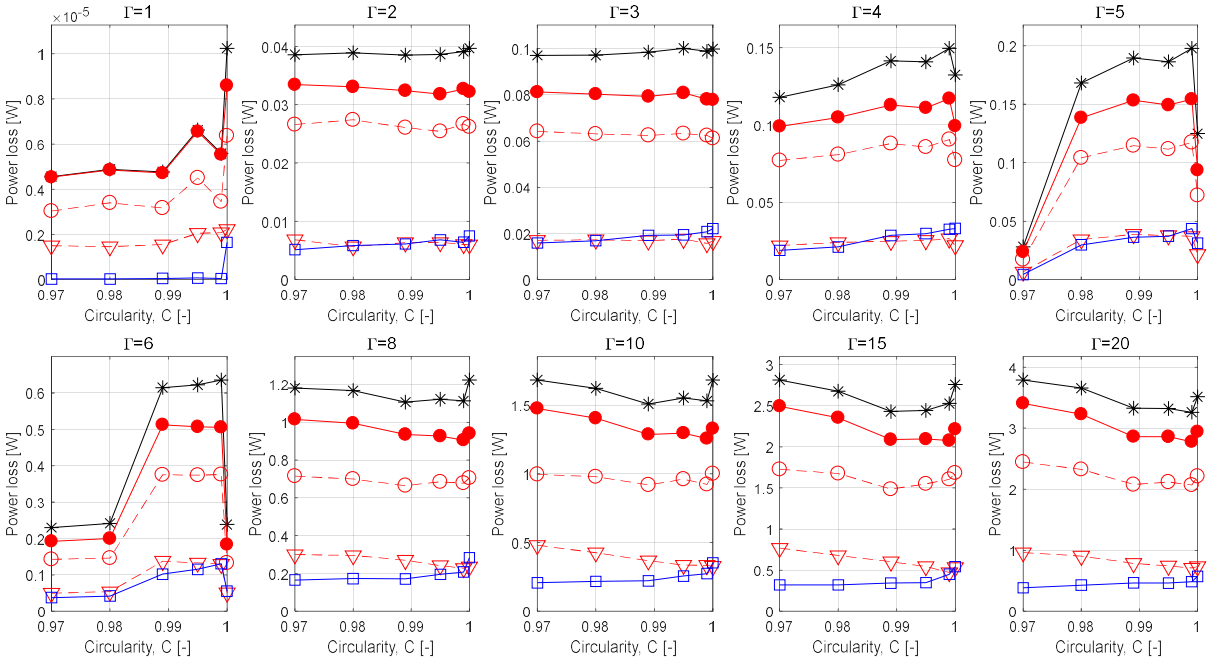

Figure 8: Power loss changes in terms of circularity at different vibration levels: total loss (—✳—), frictional loss (—●—), inter-particle frictional loss (–⊖–), particle-enclosure frictional loss (–▽–), collisional loss (—□—).

One unanticipated result is that collisional loss always increases with sphericity or circularity whatever the damping regime. It is believed that this occurs because flatter (i.e. low sphericity or low circularity) particles have fewer intense collisions (i.e. high overlap, high impact velocity). Additionally, an interesting correlation is found between collisional and particle-enclosure frictional loss characteristics along sphericity or circularity. As can be seen in Figure 7 and Figure 8, they generally have the same tendency before two-sided bouncing bed behaviour (i.e. $\Gamma < 8$) while the power loss trends of those seem opposite after this threshold vibration intensity.

5 CONCLUSIONS

This study set out to assess the effect of oblate particle usage in granular dampers undergoing vertical harmonic excitations by conducting numerical studies. The investigation has shown that the damping performance and the motional behaviour is sensitive to the sphericity level of the particles as well as the vibration amplitude. The power loss results in this study indicate that three damping regimes exist, each depends on vibration level and sphericity of the particles. Additionally, there is generally an oblate particle type which can be chosen rather than the typical perfect sphere to provide higher damping to main structures according to the motional state. Also, it has been shown that the general damping characteristics of particles follow the frictional dissipation behaviour which is the dominant mechanism in granular damping. This research extends the existing literature on damping from irregular particles. However, experimental investigations should be also conducted to confirm these numerical outcomes.

REFERENCES

[1] H. V Panossian, Non-obstructive particle damping: New experiences and capabilities, in: 49th AIAA/ASME/ASCE/AHS/ASC Struct. Struct. Dyn. Mater. Conf., Schaumburg, Illinois, 2008. doi:10.2514/6.2008-2102.

[2] H. V Panossian, Structural damping enhancement via non-obstructive particle damping technique, J. Vib. Acoust. 114 (1992) 101–105. doi:10.1115/1.2930221.

[3] S.S. Simonian, Particle beam damper, in: Proc. SPIE 2445, Smart Struct. Mater. 1995 Passiv. Damping, San Diego, California, 1995: pp. 149–160. doi:10.1117/12.208884.

[4] B.M. Shah, D. Pillet, X.M. Bai, L.M. Keer, Q. Jane Wang, R.Q. Snurr, Construction and characterization of a particle-based thrust damping system, J. Sound Vib. 326 (2009) 489–502. doi:10.1016/j.jsv.2009.06.007.

[5] Z. Xu, M. Yu Wang, T. Chen, A particle damper for vibration and noise reduction, J. Sound Vib. 270 (2004) 1033–1040. doi:10.1016/S0022-460X(03)00503-0.

[6] B. Knight, D. Parsons, A. Smith, Evaluating attenuation of vibration response using particle impact damping for a range of equipment assemblies, in: AIAA Aerosp. Des. Struct. Event, Boston, Massachusetts, 2013: pp. 1–9.

[7] Y.C. Chung, Y.R. Wu, Dynamic modeling of a gear transmission system containing damping particles using coupled multi-body dynamics and discrete element method, Nonlinear Dyn. 98 (2019) 129–149. doi:10.1007/s11071-019-05177-1.

[8] F. Duvigneau, S. Koch, E. Woschke, U. Gabbert, An effective vibration reduction concept for automotive applications based on granular-filled cavities, JVC/Journal Vib. Control. 24 (2018) 73–82. doi:10.1177/1077546316632932.

[9] J.A. Rongong, G.R. Tomlinson, Amplitude dependent behaviour in the application of particle dampers to vibrating structures, in: 46th AIAA/ASME/ASCE/AHS/ASC Struct. Struct. Dyn. Mater. Conf., Austin, Texas, 2005: pp. 6433–6441. doi:10.2514/6.2005-2327.

[10] W. Liu, G.R. Tomlinson, J.A. Rongong, The dynamic characterisation of disk geometry particle dampers, J. Sound Vib. 280 (2005) 849–861. doi:10.1016/j.jsv.2003.12.047.

[11] J.J. Hollkamp, R.W. Gordon, Experiments with particle damping, in: Proc. SPIE 3327, Smart Struct. Mater. 1998 Passiv. Damping Isol., San Diego, California, 1998: pp. 2–12. doi:10.1117/12.310675.

[12] Z. Lu, S.F. Masri, X. Lu, Parametric studies of the performance of particle dampers under harmonic excitation, Struct. Control Heal. Monit. 18 (2011) 79–98. doi:10.1002/stc.359.

[13] A. Papalou, S.F. Masri, Performance of particle dampers under random excitation, J. Vib. Acoust. 118 (1996) 614–621. doi:10.1115/1.2888343.

[14] M. Sánchez, G. Rosenthal, L.A. Pugnaloni, Universal response of optimal granular damping devices, J. Sound Vib. 331 (2012) 4389–4394. doi:10.1016/j.jsv.2012.05.001.

[15] K. Mao, M.Y. Wang, Z.Z. Xu, T. Chen, Simulation and characterization of particle

damping in transient vibrations, J. Vib. Acoust. 126 (2004) 202–211. doi:10.1115/1.1687401.

[16] C.X. Wong, M.C. Daniel, J.A. Rongong, Energy dissipation prediction of particle dampers, J. Sound Vib. 319 (2009) 91–118. doi:10.1016/j.jsv.2008.06.027.

[17] K. Mao, M.Y. Wang, Z. Xu, T. Chen, DEM simulation of particle damping, Powder Technol. 142 (2004) 154–165. doi:10.1016/j.powtec.2004.04.031.

[18] Y. Wang, B. Liu, A. Tian, W. Tang, Experimental and numerical investigations on the performance of particle dampers attached to a primary structure undergoing free vibration in the horizontal and vertical directions, J. Sound Vib. 371 (2016) 35–55. doi:10.1016/j.jsv.2016.01.056.

[19] M. Sánchez, C.M. Carlevaro, L.A. Pugnaloni, Effect of particle shape and fragmentation on the response of particle dampers, J. Vib. Control. 20 (2014) 1846–1854. doi:10.1177/1077546313480544.

[20] H. Pourtavakoli, E.J.R. Parteli, T. Pöschel, Granular dampers: Does particle shape matter?, New J. Phys. 18 (2016). doi:10.1088/1367-2630/18/7/073049.

[21] J.M. Bajkowski, B. Dyniewicz, M. Gębik-Wrona, J. Bajkowski, C.I. Bajer, Reduction of the vibration amplitudes of a harmonically excited sandwich beam with controllable core, Mech. Syst. Signal Process. 129 (2019) 54–69. doi:10.1016/j.ymssp.2019.04.024.

[22] P.A. Cundall, O.D.L. Strack, A discrete numerical model for granular assemblies, Geotechnique. 29 (1979) 47–65. doi:10.1680/geot.1979.29.1.47.

[23] B.L. Fowler, E.M. Flint, S.E. Olson, Effectiveness and predictability of particle damping, in: Proc. SPIE 3989, Smart Struct. Mater. 2000 Damping Isol., Newport Beach, California, 2000: pp. 356–367. doi:10.1117/12.384576.

[24] D. Markauskas, R. Kačianauskas, A. Džiugys, R. Navakas, Investigation of adequacy of multi-sphere approximation of elliptical particles for DEM simulations, Granul. Matter. 12 (2010) 107–123. doi:10.1007/s10035-009-0158-y.

[25] I. Cruz-Matías, D. Ayala, D. Hiller, S. Gutsch, M. Zacharias, S. Estradé, F. Peiró, Sphericity and roundness computation for particles using the extreme vertices model, J. Comput. Sci. 30 (2019) 28–40. doi:10.1016/j.jocs.2018.11.005.

[26] Y. Tatemoto, Y. Mawatari, T. Yasukawa, K. Noda, Numerical simulation of particle motion in vibrated fluidized bed, Chem. Eng. Sci. 59 (2004) 437–447. doi:10.1016/j.ces.2003.10.005.

[27] L. Vu-Quoc, X. Zhang, L. Lesburg, Normal and tangential force-displacement relations for frictional elasto-plastic contact of spheres, Int. J. Solids Struct. 38 (2001) 6455–6489. doi:10.1016/S0020-7683(01)00065-8.

[28] T. Iwasaki, M. Satoh, T. Koga, Analysis of collision energy of bead media in a high-speed elliptical-rotor-type powder mixer using the discrete element method, Powder Technol. 121 (2001) 239–248. doi:10.1016/S0032-5910(01)00384-9.

[29] Y. Tsuji, T. Tanaka, T. Ishida, Lagrangian numerical simulation of plug flow of cohesionless particles in a horizontal pipe, Powder Technol. 71 (1992) 239–250. doi:10.1016/0032-5910(92)88030-L.

[30] L. Vu-Quoc, X. Zhang, Accurate and efficient tangential force-displacement model for

elastic frictional contact in particle-flow simulations, Mech. Mater. 31 (1999) 235–269. doi:10.1016/S0167-6636(98)00064-7.

[31] EDEM, EDEM software user manual, (2020).

[32] R.D. Friend, V.K. Kinra, Particle impact damping, J. Sound Vib. 233 (2000) 93–118. doi:10.1006/jsvi.1999.2795.

[33] M. Ben Romdhane, N. Bouhaddi, M. Trigui, E. Foltête, M. Haddar, The loss factor experimental characterisation of the non-obstructive particles damping approach, Mech. Syst. Signal Process. 38 (2013) 585–600. doi:10.1016/j.ymssp.2013.02.006.

[34] B. Darabi, J.A. Rongong, Polymeric particle dampers under steady-state vertical vibrations, J. Sound Vib. 331 (2012) 3304–3316. doi:10.1016/j.jsv.2012.03.005.

[35] C.X. Wong, M.C. Daniel, J.A. Rongong, Prediction of the amplitude dependent behaviour of particle dampers, in: AIAA/ASME/ASCE/AHS/ASC Struct. Struct. Dyn. Mater. Conf., Honolulu, Hawaiii, 2007: pp. 4167–4182. doi:10.2514/6.2007-2043.